Chinese Science Bulletin

Study on flow characteristics of solid/liquid system in lysozyme crystal growth

CUI HaiLiang[1], YU Yong[1†], CHEN WanChun[1,2] & KANG Qi[1]

[1] National Microgravity Laboratory, Institute of Mechanics, Chinese Academy of Sciences, Beijing 100080, China;
[2] Institute of Physics, Chinese Academy of Sciences, Beijing 100080, China

During the process of lysozyme protein crystallization with batch method, the macroscopic flow field of solid/liquid system was observed by particle image velocimetry (PIV). Furthermore, a normal growth rate of (110) face and local flow field around a single protein crystal were obtained by a long work distance microscope. The experimental results showed that the average velocity, the maximal velocity of macroscopic solid/liquid system and the velocity of local flow field around single protein crystal were fluctuant. The effective boundary layer thickness δ_{eff}, the concentration at the interface C_i and the characteristic velocity V were calculated using a convection-diffusion model. The results showed that the growth of lysozyme crystal in this experiment was dominated by interfacial kinetics rather than bulk transport, and the function of buoyancy-driven flow in bulk transport was small, however, the effect of bulk transport in crystal growth had a tendency to increase with the increase of lysozyme concentration. The calculated results also showed that the order of magnitude of shear force was about 10^{-21} N, which was much less than the bond force between the lysozyme molecules. Therefore the shear force induced by buoyancy-driven flows cannot remove the protein molecules from the interface of crystal.

protein crystal, batch method, buoyancy-driven flows, particle image velocimetry, shear force

Obtaining large and high-quality protein single crystals is the limiting factor to determine their three-dimensional structures of protein molecules by X-ray diffraction. Mass transfer and growth kinetics have been studied to overcome this difficulty[1]. Crystallization is inherently unable to maintain a state of equilibrium as it creates a solute concentration gradient which may lead to a buoyancy-driven flow in the gravitational field[2]. The buoyancy-driven flow is thought to be detrimental to protein crystal growth, because it influences the steady-state protein concentration gradient around the growing protein crystal and destroys its mass filtering capability[3]. The flow field and concentration field around the protein crystal were observed by the interferometry[4−9] and particle tracking velocimetry techniques[3]. The simulated calculation was also used to study the influence of convection to protein crystal[10−12]. Grant[13] and Vekilov[14] stated that convection transport increases the interfacial impurity concentration, which reduces the growth rate of the crystal. In fact, the influence of convection transport on crystal growth in different growth mechanisms is unclear, which is demonstrated by experiments conducted in the space environment. It was assumed that space was the perfect environment for the production of higher quality protein crystal because the sedimentation movement and convective flow due to the gravity are negligible under microgravity conditions[15,16]. A number of experiments carried out by space aircrafts have produced some crystals that were relatively large and well ordered compared with that growth on the earth. However, there have also

Received September 16, 2006; accepted December 28, 2006
doi: 10.1007/s11434-007-0176-2
†Corresponding author (email: yuyong@imech.ac.cn)
Supported by the National Natural Science Foundation of China (Grant Nos. 10472127 and 10432060) and the Knowledge Innovation Program of Chinese Academy of Sciences (Grant Nos. KSCX2-SW-322 and KJCX2-SW-L05)

been a lot of crystals produced in space experiments that have no noticeable improvement in the quality and internal structure compared with those growing under the normal gravity on the earth[17−19]. The reasons are unknown.

In this paper, the flow fields of solution in which the lysozyme crystal grew were obtained by using particle image velocimetry (PIV) technology. The growth rates were determined by using a long work distance microscopy. The influence of convection transport for the growth of lysozyme crystal was studied by analyzing those data.

1 Experiments

1.1 Materials

The buffer solution was HAC-NaAC solution (50 mmol/L, pH 4.5). Chicken egg-white lysozyme was purchased from Sigma. All other reagents were of analytical grade. Distilled water was used.

1.2 Instruments

Long work distance microscope (made in America by Questar Company) and particle imaging velocimetry (made in Danmark by Dantec Company).

1.3 Experimental

1.3.1 Lysozyme crystal growth with batch method. An amount of lysozyme powder and NaCl were dissolved in the buffer solution respectively. Those solutions were kept at 4℃. The upper clear lysozyme solution was mixed with the same volume of NaCl solution in a cell to produce protein crystals. The size of cell was 10 mm×10 mm×10 mm. The initial protein concentrations were from 25 to 55 mg/mL (the equilibrium saturation concentration of lysozyme C_S is 9.23 mg/mL in 28℃).

1.3.2 Flow field measurements. Particle image velocimetry (PIV) was used to observe the macroscopical flow field as shown in Figure 1. Some tracer particles were put into NaCl solution. After being churned, the solution was mixed with the same volume of lysozyme solution in a cell. The cell was illuminated by double pulsed Nd:YAG laser at 532 nm wavelength. The interval between two pulses was 2.5 s. Some part of the planar light reflected by tracer particles was recorded in CCD. The displacement vector was obtained by analyzing the cross correlation of the input images. Then the flow field was calculated with the time interval between the images captures.

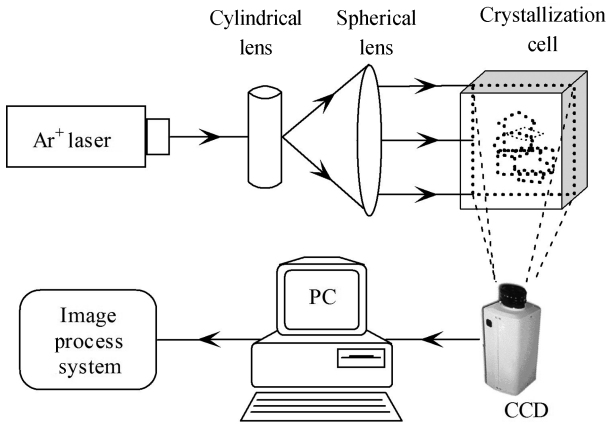

Figure 1 The diagram of PIV used in the macroscopical flow field measurements.

1.3.3 The growth rates of lysozyme crystal (110) face and local flow field measurements. Growth kinetic curve indicates the kinetic process of protein crystal growth by showing the relationship between the face normal growth rate of crystal and time. A cold light (LED) was used as the microscopic light illumination. At first, some 10 μm tracer particles were put into solution. The movement of a few tracer particles and many translucent particles was found when the face normal growth rate was obtained with long work distance microscope as shown in Figure 2. It was possible that the translucent particles were crystal nuclei or aggregates in solutions. Because the sizes of the translucent particles were only about several microns, they could show the movement of the solution. The local flow field would be obtained from two sequential pictures with PIV technique.

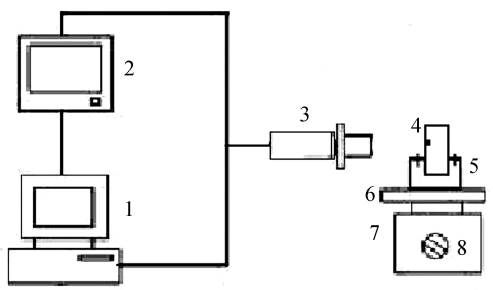

Figure 2 The diagram of crystal observation with long work distance microscope. 1, Computer; 2, monitor; 3, long work distance microscope; 4, single protein crystal; 5, crystallizing cell; 6, swivel plate; 7, swivel groupware; 8, joy stick.

2 Model of calculating characteristic parameters of crystal growth

Protein crystal growth may be approximately figured as a two-step process[20]. In the first step, protein molecules move from the solution to the crystal interface. The mass flux is described by Fick First Law:

$$\dot{m}_T = D\nabla C \approx \frac{D(C_\infty - C_\mathrm{i})}{\delta_\mathrm{eff}}, \tag{1}$$

where D is the diffusion coefficient, C_∞ is the main concentration, C_i is the concentration of solid/liquid interface, and δ_eff is the effective boundary layer thickness.

In the second step, protein molecules move from the crystal interface to the crystalline lattice. The mass flux transported is

$$\dot{m}_S = k\left[\left(C_\mathrm{i} - C_\mathrm{S}\right)/C_\mathrm{S}\right]^\beta, \tag{2}$$

where k, β are kinetic parameters of growth, and C_S is the equilibrium saturation concentration, and the relation between growth rate and mass flux is

$$R = \dot{m}_S/(C_x - C_i), \tag{3}$$

where R is the face normal growth rate of crystal, C_X is the concentration of solute in the crystal. Due to conservation of mass, namely $\dot{m}_S = \dot{m}_T$, eqs. (4) and (5) are obtained.

$$R(C_X - C_\mathrm{i}) = D(C_\infty - C_\mathrm{i})/\delta_\mathrm{eff}, \tag{4}$$

$$R(C_X - C_\mathrm{i}) = k[(C_\mathrm{i} - C_\mathrm{S})/C_\mathrm{S}]^\beta, \tag{5}$$

C_∞, C_S and C_X could be known in advance, except C_i. The face normal growth rate R can be observed under various C_∞. If the effective boundary layer thickness δ_eff can be achieved, we should calculate C_i from eq. (4) and k, β from eq. (5).

The effective boundary layer thickness δ_eff can be predicted from a simple fluid mechanical model. After the steady flow is supposed and the advection term is neglected, the momentum equation including only vertical component of velocity can be transformed into

$$g\frac{\Delta\rho}{\rho} = \upsilon\frac{\mathrm{d}^2 v_Z}{\mathrm{d}y^2} \approx \upsilon\frac{v_Z}{\delta_\mathrm{C}^2}, \tag{6}$$

where g is the acceleration of gravity, υ is the kinetic viscosity, and $g\Delta\rho$ is the buoyancy from density difference $\Delta\rho$, δ_c is the convective boundary layer thickness, and v_Z can be obtained from eq. (7),

$$v_Z = DL/\delta_C^2. \tag{7}$$

Substituting eq. (7) into eq. (6), eq. (8) holds:

$$\delta_\mathrm{C}^2 = \frac{\upsilon v_Z}{g\Delta\rho/\rho}, \tag{8}$$

where $\Delta\rho/\rho$ depends on C_i, and the relation can be given by eq. (9) on the interface of crystal.

$$\frac{\Delta\rho}{\rho} = \frac{\left(C_\infty - C_\mathrm{i}\right)\left(\rho_\mathrm{A} - \rho_\mathrm{B}\right)}{\rho_\mathrm{A}\rho_\mathrm{B} + C_\infty\left(\rho_\mathrm{A} - \rho_\mathrm{B}\right)}. \tag{9}$$

And δ_eff can be calculated by the convective transport as expressed in eq. (10),

$$\delta_\mathrm{eff}^{-1} = a^{-1} + \delta_\mathrm{c}^{-1}, \tag{10}$$

where a is the radius of the crystal (a is set as $L/2$).

With the measurements of the growth rate R, the radius of crystal a and the concentration of solution C_∞, the characteristic velocity of solution convection V (namely v_Z in eq. (7)), the effective boundary layer thickness δ_eff and the concentration at the interface C_i can be calculated from iteration of eqs. (4), (5), (7)—(10).

3 Results and discussion

3.1 Growth kinetic curves

Series of experiments of lysozyme crystal growth with batch method were performed. The ambient temperature is 28℃. The initial protein concentrations in experiments are shown in Table 1, where supersaturation $\sigma = \frac{C_\infty - C_\mathrm{S}}{C_\mathrm{S}}$. Protein crystal growth kinetic curves were derived from the size of crystal with time.

Table 1 The supersaturation of lysozyme crystal solutions (28℃)

C_∞ (mg/mL)	25	35	40	41.25	42	42.5	43.5	45	50	55
σ	1.71	2.79	3.33	3.47	3.55	3.60	3.74	3.87	4.41	4.96

At 50 mmol/L HAC-NaAC, 7% NaCl and 28℃, the crystal size a of lysozyme crystal (110 face) with time is shown in Figure 3. The normal growing rates of lysozyme crystal (110) face with time are shown in Figure 4. The experiments showed that the growth rates of (110) face increased with increase of the supersaturation and decreased with time tardily because of the decrease of protein concentration in solution, which resulted from the crystal growth.

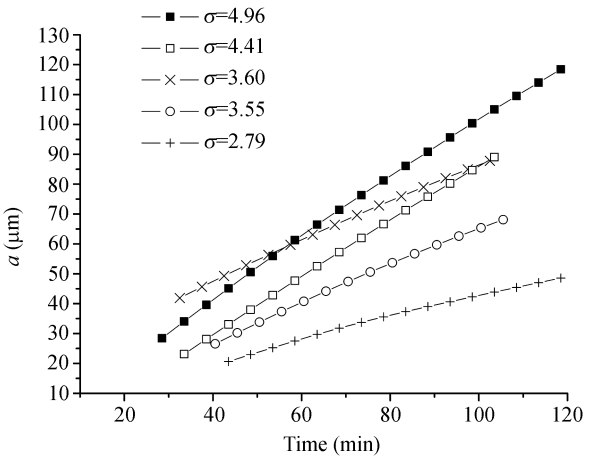

Figure 3 The graph of crystal size with time. 50 mmol/L HAC-NaAC, 7% NaCl, 28℃.

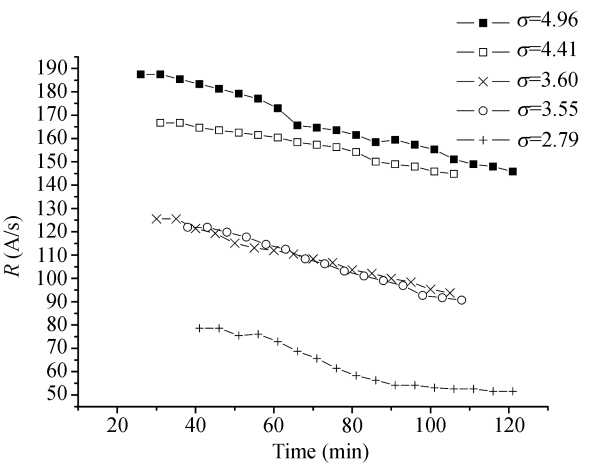

Figure 4 The kinetic curve (of 110 face) of lysozyme crystal growth, R is the growth rate of (110) face. 50 mmol/L HAC-NaAC, 7% NaCl, 28℃.

3.2 The flow field of solution during lysozyme crystal growth

3.2.1 The macroscopic flow field of bulk solution. The macroscopic flow field of bulk solution during lysozyme crystal growth under various supersaturation σ was observed by using PIV method. In Figure 5, (a) shows a raw picture and (b) shows the flow field after (a) was analyzed with PIV technology.

There were a lot of small crystals accumulating on the bottom of the cell after some time from crystal growth start-up. Small crystal growth consumed lysozyme molecules in solute, which made the protein concentration on the bottom lower than that above. Hence buoyancy flow was induced by a concentration gradient as shown in Figure 5(b).

The average velocity V_a revealing flow intensity could be obtained by averaging the volume of all the velocity in flow field. The variation of V_a with time under those supersaturations listed in Table 1 was obtained. Figure 6 shows the variation of V_a with time under the four supersaturations. The flow intensity had no distinct changes as $\sigma < 3.33$, but increased obviously as $\sigma > 3.55$. In general, the flow intensity increased with the increase of the supersaturation.

Considering that flow intensity changed with positions, the maximal velocity at 300 μm above the cell bottom was selected as V_{bot}. Figure 7 shows the variation of V_{bot} with time. It was easy to find that the change tendencies of V_{bot} and V_a with time were accordant basically by analyzing Figure 7 and Figure 6 together.

3.2.2 Local flow field around a single crystal. The local flow field around a single protein crystal was observed and shot by the long work distance microscope. The local velocity field could be obtained with the analysis of PIV technology on the flow pictures recorded. The 2D velocity field shown in Figure 8 paralleled the direction of gravity, because the single crystal was adhered to the wall perpendicular to the horizontal plane.

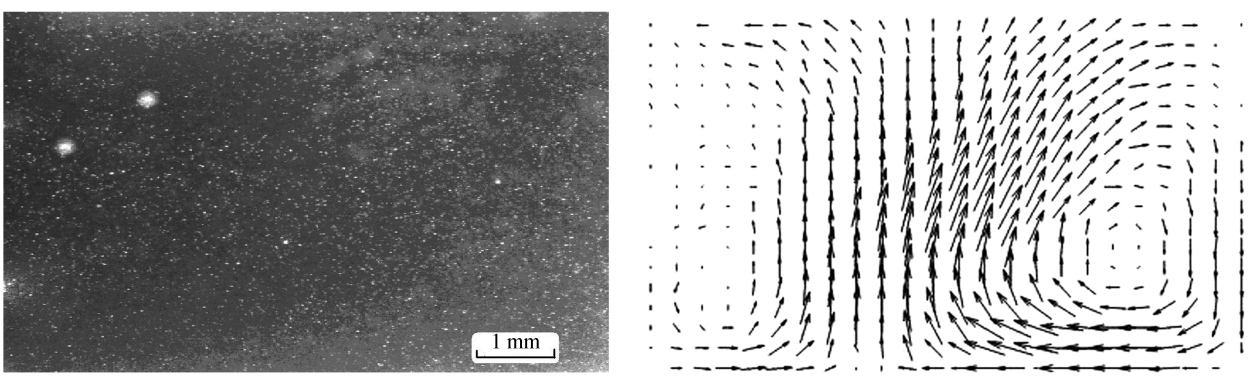

Figure 5 PIV pictures. 50 mmol/L HAC-NaAC, 7% NaCl, 28℃, σ =3.87. (a) The raw picture was obtained after lysozyme and NaCl solutions were mixed for 20 min; (b) the flow field with analysis of PIV technology on (a).

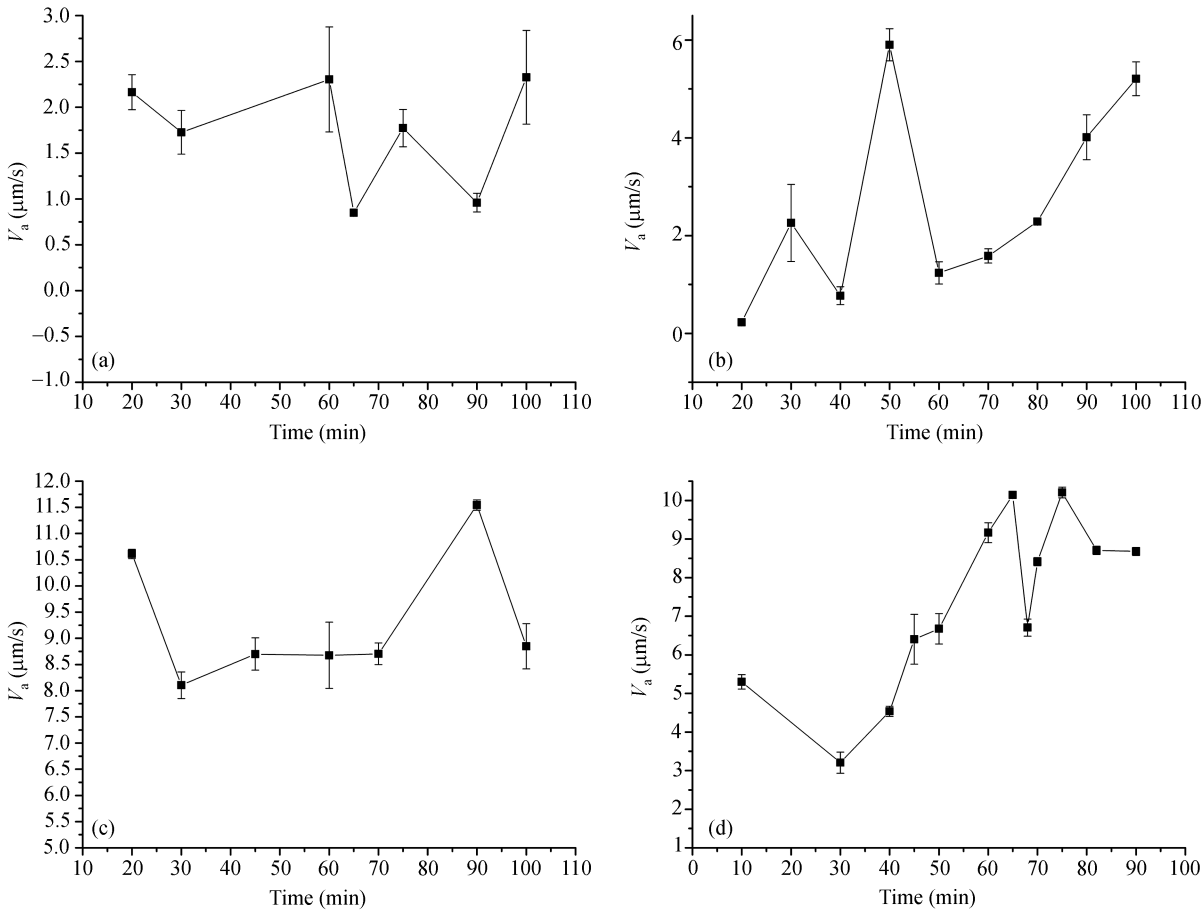

Figure 6 The average velocity in the cell with time. 50 mmol/L HAC-NaAC, 7% NaCl, 28℃. (a) σ=3.33; (b) σ=3.55; (c) σ=3.87; (d) σ=4.41.

Figure 9 shows the variation of the maximal velocity V_s in the field of vision with time under $\sigma = 4.41$. The results displayed that the flow rates of the local flow field was fluctuant and the local flow velocity V_s was larger than the average velocity V_a (Figure 6) and the maximal velocity V_{bot} (Figure 7) in cell .

It was inferred from Figures 6, 7, 9 that the flow was not steady but variable using batch method to grow crystals. However, the complex solution flow could not affect the growth rate of (110) face significantly because the growth rates of (110) face decreased with decreasing time so slowly.

3.3 The characteristic speed, the effective boundary layer thickness, and the concentration at the interface

The effective boundary layer thickness δ_{eff}, the characteristic speed of solution convection V, and the concentration at the interface C_i were calculated from iteration of eqs. (4), (5), (7)—(10) with the measurements of the growth rate R, the radius of crystal a and the solution concentration C_∞. Other parameters of physical properties were[20]: $D = 1.00\times10^{-6}$ cm^2/s, ν=1×10^{-2} cm^2/s, C_X=0.927 g/cm^3, $k = 1.11\times10^{-9}$ cm/s, $\beta = 2.08$.

The function of convection in bulk transport was studied with the curve of $\delta_{eff}/a \sim L$ as shown in Figure 10. Based on crystal growth kinetics theory, if $\delta_{eff} \approx a$, bulk transport is dominated by diffusion; if δ_{eff}/a gets smaller, the function of convective transport became larger[20]. For the values of δ_{eff}/a were less than one and decreased rapidly with the increase of L and σ in Figure 10, the function of the convective transport increased with the increase of L and σ.

The relative importance of interfacial kinetics and bulk transport was analyzed with the curve of $\lambda = (C_i - C_S)/(C_\infty - C_S) \sim L$ as shown in Figure 11. If $C_i \approx C_\infty$, namely $\lambda \approx 1$, crystal growth is dominated by interfacial kinetics; if $C_i \approx C_S$, namely $\lambda \approx 0$, crystal

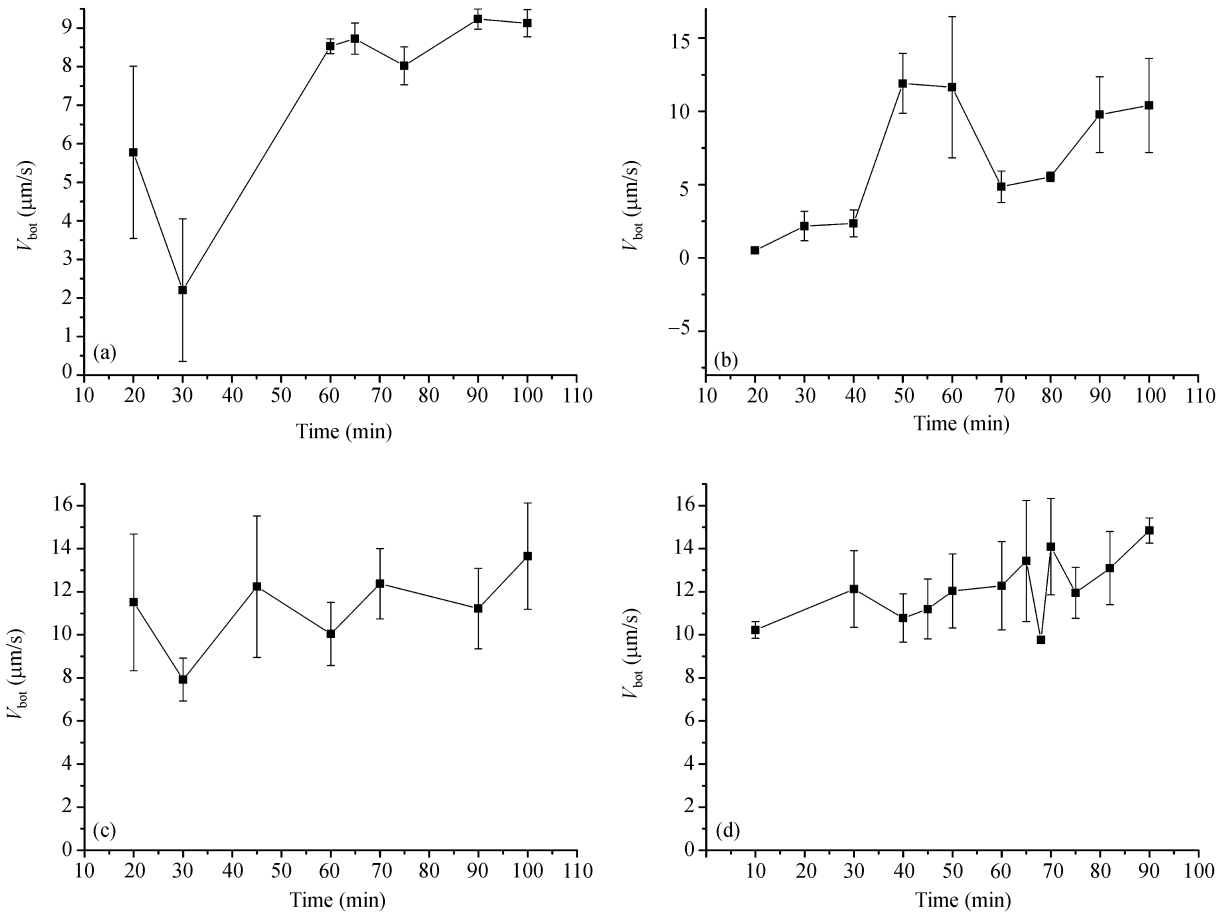

Figure 7 The maximal velocity V_{bot} with time. 50 mmol/L HAC-NaAC, 7% NaCl, 28℃. (a) σ=3.33; (b) σ=3.55; (c) σ=3.87; (d) σ=4.41.

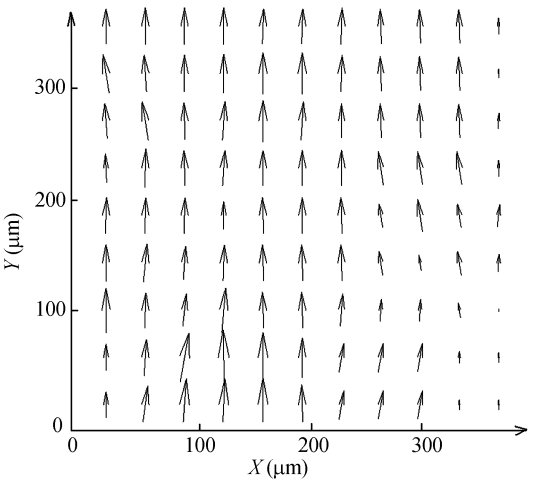

Figure 8 The local velocity field obtained with PIV technology.

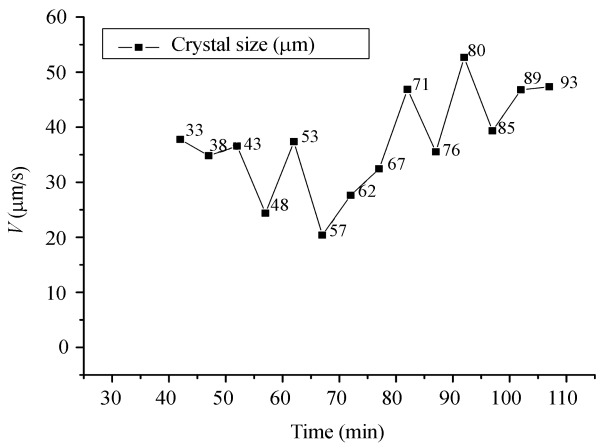

Figure 9 The local maximal speed V_s around a single crystal. σ =4.41, 50 mmol/L HAC-NaAC, 7% NaCl, 28℃.

growth is dominated by bulk transport. The solution concentration C_∞decreased with decreasing time gradually, but very slowly. Therefore we used the initial solution concentration instead of the real concentration. It was inferred that crystal growth was dominated by interfacial kinetics in the experiments because λ was larger than 1/2 and close to 1 in Figure 11. This result accorded with the conclusion above in section 3.2. Simultaneously, though the importance of bulk transport was less in the experiments, it also affected crystal growth. The value of λ decreased with the increase of σ in Figure 11, so the relative importance of bulk trans-

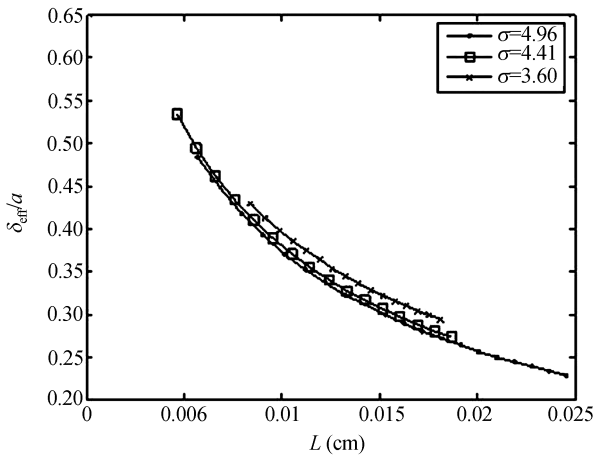

Figure 10 The values of δ_{eff}/a against L under various σ. 50 mmol/L HAC-NaAC, 7% NaCl, 28℃.

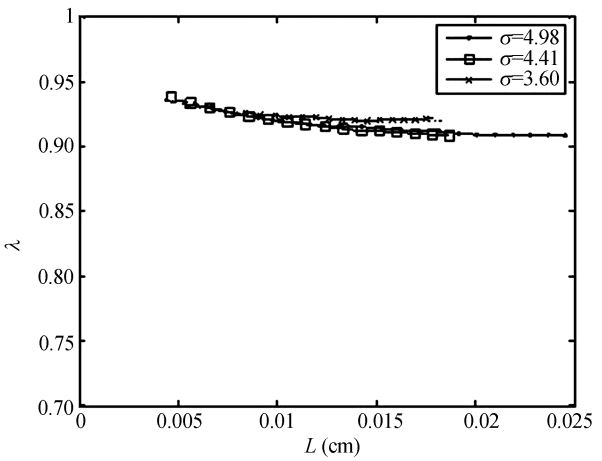

Figure 11 λ against L under various σ. 50 mmol/L HAC-NaAC, 7% NaCl, 28℃.

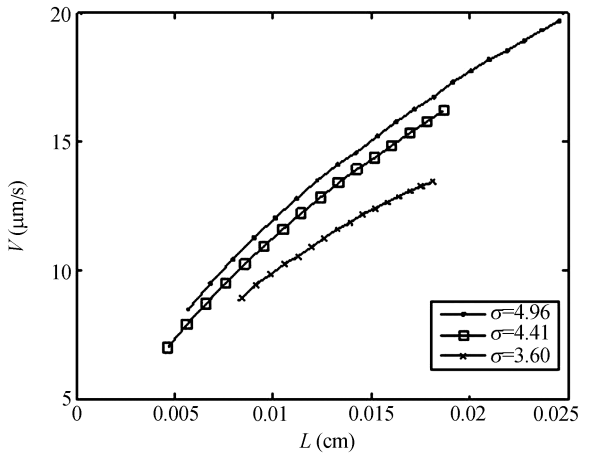

Figure 12 V against L under various σ. 50 mmol/L HAC-NaAC, 7% NaCl, 28℃.

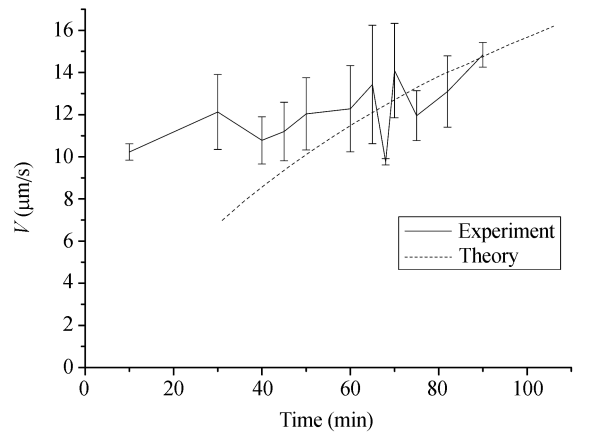

Figure 13 Experimental maximal speed V_{bot} and characteristic speed V. σ= 4.41 (dash line is V, solid line is V_{bot}).

port increased with the increase of σ. At large σ, the growth rate of crystal might be affected by the fluctuant flow rates, because: 1) the local velocity field around a single crystal was fluctuant as shown Figure 9; 2) the influence of flow field around crystal to the growth rate could not be neglected due to the function of bulk transport gets larger. Therefore, the computed results were coincident with the experiments.

The characteristic velocity V against L is shown in Figure 12, implying that V increased with the increase of crystal size. The experimental maximal speed V_{bot} was compared with the characteristic speed V computed from the convection-diffusion model in Figure 13. It was proved that the model used in the paper could describe the flow field around growing lysozyme crystals reasonably because of the accordant tendency of two values in Figure 13.

3.4 The effects of shear force of convection on crystal growth

Weak hydrogen bond, Van de Waal force and Coulomb force are the main parts of the force between protein molecules. The Coulomb force between protein molecules is much less than the force of electrovalent bond in an inorganic crystal. The force between protein molecules is small, which may be less than the shear force induced by natural convection[13]. If the shear force is larger, protein molecules might be divested of the crystal interface or growing step. The shear force was estimated in order to judge whether it affected crystal growth.

The intensity of natural convection induced by density difference is denoted by Grashof number (Gr), which is the ratio of buoyancy force and viscous drag. Schmidt number (Sc) is the ratio of the molecular transport coefficients for momentum and diffusion.

$$\mathrm{Gr} = a^3 g \Delta\rho / \rho\upsilon^2 , \quad (11)$$

$$\mathrm{Sc} = \nu / D . \quad (12)$$

Gr was less than 0.01 and Sc was 10^4 in the experiment. Shear fore could be calculated with eq. (13) for small Gr and large Sc [13]. Substituting the effective boundary layer thickness δ_{eff} and the characteristic velocity V iterated from eqs. (4), (5), (7)—(10) for δ, V in eq. (13), the curve of shear force against crystal size L was obtained as shown in Figure 14.

$$\tau = \mu\Gamma = \mu V / \delta = \rho\upsilon V / \delta, \quad (13)$$

where τ is the shear force, μ is the fluid viscosity, Γ is the shear rate, V is the characteristic velocity, δ is boundary layer thickness, ρ is the fluid density, and υ is the kinetic viscosity.

The order of magnitude of the shear force in the solution was 10^{-21} N as shown in Figure 14. The shear force was much less than the force to break the bond between lysozyme molecules which was F=8.3×10^{-13} N [13], hence the shear force cannot remove the protein molecules from the interface of crystal, which is in agreement with the calculated result in ref. [13].

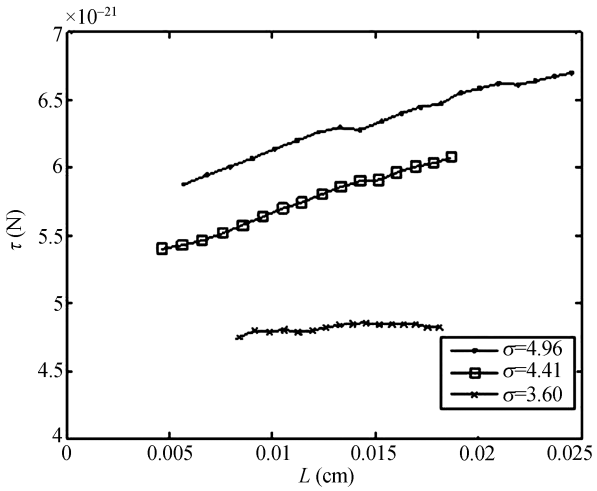

Figure 14 Shear force τ against crystal size L. 50 mmol/L HAC-NaAC, 7% NaCl, 28℃.

4 Conclusions

There were visible buoyancy convections in solution when lysozyme crystals were made with batch method. The macroscopic velocity in solution and local velocity around crystals were characterized by their fluctuation. The intensity of local flow field was larger than that of macroscopic flow field.

The growth of lysozyme in this experiment was dominated by interfacial kinetics rather than bulk transport. But the relative importance of bulk transport in crystal growth had a tendency to increase with the increase of concentration. Under a high supersaturation condition, the influence of local flow field around the crystal would enhance the growth rate, and potentially make it more highly variable. The calculated results also showed that the order of magnitude of shear force was 10^{-21} N, which was much less than the bond force between the lysozyme molecules. Therefore, the shear force induced by buoyancy-driven flows cannot remove the protein molecules from the interface of crystal.

The authors would like to thank Dr. Hong Liu and Gloria Witkus at University of Florida IFAS, C/O USDA, ARS Invasive Plant Research Laboratory.

1 Miyashita S, Romatso H, Suzuki Y, et al. Observation of the concentration distribution around a growing lysozyme crystal. J Cryst Growth, 1994, 141(3-4): 419—424
2 Pusey M, Witherow W, Naumann R. Preliminary investigations into solutal flow about growing tetragonal lysozyme crystals. J Cryst Growth, 1988, 90(1-3): 105—111
3 Kawaji M, Gamache O, Hwang D H, et al. Investigation of Marangoni and natural convection during protein crystal growth. J Cryst Growth, 2003, 258(3-4): 420—430
4 Vekilov P G, Ataka M, Katsura T. Laser Michelson interferometry investigation of protein crystal growth. J Cryst Growth, 1993, 130(1-2): 317—320
5 Kuznetsov Y G, Malkin A J, Greenwood A, et al. Michelson interferometric studies of protein and virus crystal growth. J Cryst Growth, 1996, 166(1-4): 913—918
6 Vekilov P G, Monaco L A, Rosenberger F. High resolution interferometric technique for *in-situ* studies of crystal growth morphologies and kinetics. J Cryst Growth, 1995, 148(3): 289—296
7 Kuznetsov Y G, Malkin A J, Greenwood A, et al. Interometric studies of growth kinetics and surface morphology in macromolecular crystal growth: canavalin: thaumatin, and turnip yellow mosaic virus. J Struct Biol, 1995, 114(3): 184—196
8 Otalora F, Novella M L, Gavira J A, et al. Experimental evidence for the stability of the depletion zone around a growing protein crystal under microgravity. Acta Crystallogr, 2001, D57: 412—417
9 Duan L, Kang Q, Hu W R, et al. The mass transfer process and growth rate of protein crystals. Biophys Chem, 2002, 97(2-3): 189—201
10 Bessho Y, Ataka M, Asai M, et al. Analysis of the crystallization kinetics of lysozyme using a model with polynuclear growth mecha-

nism. Biophys J, 1994, 66: 310－313
11 Lin H, Rosenberger F, Alexander J I, et al. Convective-diffusive transport in protein crystal growth. J Cryst Growth, 1995, 151(1-2): 153－162
12 Qi J, Wakayama N I. Solute convection during the whole process of protein crystal growth. J Cryst Growth, 2000, 219(4): 465－476
13 Grant M L, Saville D A. The role of transport phenomena in protein crystal growth. J Cryst Growth, 1991, 108(1-2): 8－18
14 Vekilov P G, Rosenberger F. Protein crystal growth under forced solution flow: experimental setup and general response of lysozyme. J cryst Growth, 1998, 186(1-2), 251－261
15 McPherson A. Crystallization of Biological Macromolecules. Cold Spring Harbor, New York: Cold Spring Harbor Laboratory Press, 1999. 437－450
16 Bi R C. Space crystal growth of proteins with domestic facility. Chin J Space Sci (in Chinese), 1996, 16(3): 208－215
17 Delucas L J, Smith C D, et al. Protein crystal growth aboard the U.S. space shuttle flights STS-31 and STS-32. Adv Space Res, 1992, 12(1): 393－400
18 Bi R C, Gui L L, Shi K, et al. Protein crytal growth in microgravity. Sci China Ser B-Chem, 1994, 37(10): 1185－1191
19 Bhattacharjee P, Riahi D N. Effect of rotation on surface tension driven flow during protein crystallization. Microgravity Sci Tec, 2003, XIV/4: 36
20 Pusey M, Naumann R. Growth kinetics of tetragonal lysozyme crystals. J Cryst Growth, 1986, 76(3): 593－599